

LEARNING NEUTRINO EFFECTS IN COSMOLOGY WITH CONVOLUTIONAL NEURAL NETWORKS

ELENA GIUSARMA^{1,2†}, MAURICIO REYES HURTADO², FRANCISCO VILLAESCUSA-NAVARRO^{1,3}, SIYU HE¹, SHIRLEY HO^{1,3},
CHANGHOON HAHN^{4,5}

¹Center for Computational Astrophysics, Flatiron Institute, 162 5th Avenue, 10010, New York, NY, USA

²Department of Physics, Michigan Technological University, Houghton, MI, USA

³Department of Astrophysical Sciences, Princeton University, Peyton Hall, Princeton NJ 08544-0010, USA

⁴Lawrence Berkeley National Laboratory, 1 Cyclotron Rd, Berkeley CA 94720, USA and

⁵Berkeley Center for Cosmological Physics, University of California, Berkeley CA 94720, USA

Draft version October 11, 2019

ABSTRACT

Measuring the sum of the three active neutrino masses, M_ν , is one of the most important challenges in modern cosmology. Massive neutrinos imprint characteristic signatures on several cosmological observables in particular on the large-scale structure of the Universe. In order to maximize the information that can be retrieved from galaxy surveys, accurate theoretical predictions in the non-linear regime are needed. Currently, one way to achieve those predictions is by running cosmological numerical simulations. Unfortunately, producing those simulations requires high computational resources – seven hundred CPU hours for each neutrino mass case. In this work, we propose a new method, based on a deep learning network (U-Net), to quickly generate simulations with massive neutrinos from standard Λ CDM simulations without neutrinos. We computed multiple relevant statistical measures of deep-learning generated simulations, and conclude that our method accurately reproduces the 3-dimensional spatial distribution of matter down to non-linear scales: $k < 0.7 h/\text{Mpc}$. Finally, our method allows us to generate massive neutrino simulations 10,000 times faster than the traditional methods.

Keywords: large-scale structure – neutrino cosmology – deep learning

1. INTRODUCTION

The measurement of the mass and the ordering of neutrinos, constitutes the necessary steps to understand the physics of those particles and the beyond Standard Model mechanism. The discovery of neutrino oscillations (Fukuda et al. 1998; Ahmad et al. 2002; Araki et al. 2005; Adamson et al. 2008; Ahn et al. 2012; Abe et al. 2012, 2014; Forero et al. 2014) have robustly established that at least two neutrino families are massive. However, oscillation experiments only provide bounds on the neutrino mass squared differences. In the minimal neutrino scenario, the best fit values for the solar and atmospheric mass splitting are $\Delta m_{21}^2 \equiv m_2^2 - m_1^2 \simeq 7.6 \times 10^{-5} \text{ eV}^2$ and $|\Delta m_{31}^2| \equiv |m_3^2 - m_1^2| \simeq 2.5 \times 10^{-3} \text{ eV}^2$ (Gonzalez-Garcia et al. 2014; Forero et al. 2014; Esteban et al. 2017). Since the sign of the atmospheric mass splitting is still unknown, we have two possible orderings of neutrino masses: normal ($\Delta m_{31}^2 > 0$) and inverted ($\Delta m_{31}^2 < 0$). The lower limits on the sum of neutrino masses set by oscillation experiments are $M_\nu \gtrsim 0.06 \text{ eV}$ in the normal hierarchy and $M_\nu \gtrsim 0.1 \text{ eV}$ in the inverted hierarchy. The study of the endpoint energy of electrons produced in β -decay places an upper limit on the total neutrino mass at the level of $M_\nu \lesssim 1.1 \text{ eV}$ (Kraus et al. 2005; Aker et al. 2019).

Cosmology provides an independent tool to constrain the neutrino masses and ordering. Neutrinos are the second most abundant particles in the Universe, after photons, and leave distinctive signatures on several cosmological observables. They strongly affect the background evolution of the Universe, as well as the evolution of

cosmological perturbations. The light massive neutrinos are relativistic in the early Universe and contribute to the radiation energy density. At late time, they became non-relativistic², contributing to the total matter density of the Universe. The non-relativistic neutrinos behave as Hot Dark Matter (HDM), possessing relatively large thermal velocities compared to any other massive particles. They thus cluster only on scales larger than their free-streaming length³, suppressing the growth of perturbations on smaller scales. The presence of massive neutrinos also affects the anisotropies of the Cosmic Microwave Background (CMB), as these particles may turn non-relativistic around the decoupling period, and gravitational lensing of the CMB. The current upper bound on M_ν is obtained by combining different cosmological data. In particular, the tightest constraints on M_ν , which arise by combining CMB temperature and polarization anisotropies measurements with different observations of the large-scale structure of the Universe, range from 0.22 eV to 0.12 eV at 95% confidence level (Palanque-Desabrouille et al. 2015; Giusarma et al. 2016; Vagnozzi et al. 2017; Zennaro et al. 2018; Giusarma et al. 2018; Planck Collaboration et al. 2018, 2019).

Future cosmological surveys, such as Euclid, DESI, WFIRST, LSST, and CMB-S4, are expected to improve the constraints on the cosmological parameters. In particular, upcoming galaxy surveys will provide one of the most important sources of information to determine the

² The neutrino non-relativistic transition takes place at $1+z_{\text{nr}} \simeq 1890(m_\nu/1) \text{ eV}$.

³ The free-streaming scale is defined as the scale below which the growth of neutrino perturbations is strongly suppressed. It can be written as: $k_s \simeq 0.018\sqrt{\Omega_m}(M_\nu/1\text{eV})^{1/2} h/\text{Mpc}$.

[†] egiusarm@mtu.edu

neutrino masses and their mass ordering. To achieve those goals, accurate theoretical predictions for the spatial distribution of matter and luminous tracers in the presence of massive neutrino will be crucial. A powerful tool to obtain rigorous predictions in cosmology is through cosmological simulations. In particular, N-body simulations are numerical simulations where cosmological matter fluctuations are evolved under only gravity. They allow us to make comparisons between observations and theory. They are used to generate mock galaxy catalogs and to compute covariance matrices. Lastly, they are also used to optimize observational strategies. Over the past years, a large number of N-body simulations, including massive neutrinos, have been proposed and developed in the literature. Those simulations have made it possible to study the impact of neutrino masses on clustering in fully non-linear scale in real-space (Bird et al. 2012; Lesgourgues & Pastor 2012; Villaescusa-Navarro et al. 2013; Villaescusa-Navarro et al. 2014; Peloso et al. 2015), on clustering and abundance of halo and cosmic voids (Castorina et al. 2014; Castorina et al. 2015; Massara et al. 2015) and finally on clustering of matter in redshift-space (Villaescusa-Navarro et al. 2018; Bel et al. 2019). However, simulations are computationally expensive. The development of new computational methods is thus needed to accelerate this process.

In the last decade, deep learning approaches have been applied to many different fields of research, achieving outstanding results; especially in computer vision and image recognition challenges (Krizhevsky et al. 2012). Deep learning is a branch of machine learning that makes use of deep neural networks. An increasing number of studies are also adopting these methods for a variety of problems in cosmology. For example, Ravanbakhsh et al. (2017) and He et al. (2018) applied convolutional neural networks (CNNs) to estimate the cosmological parameters directly from simulated dark matter distributions and the distribution of photons in Cosmic Microwave Background; He et al. (2019) built a deep CNN to predict the non-linear structure formation of the Universe from simple linear perturbation theory; Rodriguez et al. (2018) and Zamudio-Fernandez et al. (2019) used Generative Adversarial Networks (GANs) models to synthesize samples of the cosmic web and predict high-resolution 3D distributions of cosmic neutral hydrogen; finally, Hezaveh et al. (2017) exploited the use of CNNs to estimate the strong gravitational lensing parameters accurately.

In this paper, we apply a modified version of the deep neural network proposed by He et al. (2019) to establish the mapping between simulations with massless and massive neutrinos. The important advantage of our approach consists in the ability to produce complex numerical simulations from the standard ones in an extremely fast way and with high accuracy.

The paper is organized as follows. In Section 2 we briefly describe the cosmological simulations we have used in this work. We then present our model’s architecture and the quantitative results in Sections 3 and 4. Finally, we draw our conclusions in Section 5.

2. N-BODY SIMULATION DATA

In this section, we briefly describe the N-body simulations used in our work. We refer the reader to Villaescusa-Navarro et al. (2018); Villaescusa-Navarro

et al. (2019) for further details on the simulations.

We use two subsets of HADES simulations (Villaescusa-Navarro et al. 2018), the precursor of the QUIJOTE simulations (Villaescusa-Navarro et al. 2019): the standard, Λ CDM, simulations (without neutrinos), and simulations with massive neutrinos. The value of the cosmological parameters are: $\Omega_m = \Omega_{\text{cdm}} + \Omega_b + \Omega_\nu = 0.3175$, $\Omega_b = 0.049$, $h = 0.6711$, $\Omega_\Lambda = 0.6825$, $n_s = 0.9624$ and $A_s = 2.13$. The simulations with massive neutrinos have $M_\nu = 0.15$ eV, and since A_s is fixed in both sets, the value of σ_8 is different: $\sigma_8 = 0.833$, and $\sigma_8 = 0.798$ for 0.0 eV and 0.15 eV neutrinos. All the simulations are run in a periodic box size of $1 h^{-1}\text{Gpc}$ and follow the evolution of the cold dark matter (CDM) and neutrino particles (only in the case of simulations with massive neutrinos), from $z = 99$ to $z = 0$. We use 100 independent realizations for each model, containing the same number of cold dark matter and neutrino particles ($N_{\text{cdm}} = N_\nu = 512^3$). We focus our analysis at redshift $z = 0$, corresponding to the present time.

In order to speed up the process of training the neural network and to avoid GPUs memory problems, we split each of the 100 simulations into sub-cubes of size 32^3 voxels in Lagrangian space⁴, corresponding to a volume of $62.5h^{-1}\text{Mpc}$ on each side. Each realization contains thus 4,096 sub-cubes, making a total of 409,600 voxels for each simulation model. We then split the realizations of each model into three chunks: 70% for training (70 realizations), 20% for validation (20 realizations) and 10% (10 realizations) for testing. After the training and the testing, we concatenate the sub-cubes of each of the 10 realizations in the test data in a cube of size $1 h^{-1}\text{Gpc}$ and we compute the relevant summary statistics.

3. METHOD

In this section, we introduce the deep neural network architecture used in our analysis to generate N-body simulations with massive neutrinos from standard Λ CDM simulations.

3.1. Network Architecture

We use a modified version of the deep neural network, Deep Density Displacement Model (D^3M), introduced by He et al. (2019). D^3M is a generalization of the standard U-Net, first proposed in Ronneberger et al. (2015) for biomedical image segmentation, to work with three-dimensional data. The network architecture is illustrated in Figure 1. It consists of a *contracting path* and an *expansive path*. The contracting path follows the typical architecture of a convolutional neural network, and it includes two blocks. Each block consists of the repeated application of two convolutions with stride 1 and a down-sampling convolution with stride 2 each followed by batch normalization (BN) and a rectified linear unit (ReLU). For each convolutional layer, we use $3 \times 3 \times 3$ filters, and we apply a zero padding with size 1. At each down-sampling step, we reduce the spatial information by half, and we increase by double the number of feature channels. The bottom of the U-Net consists of two convolutional neural networks followed by the same

⁴ Notice that the initial conditions of our simulations are generated from a regular grid.

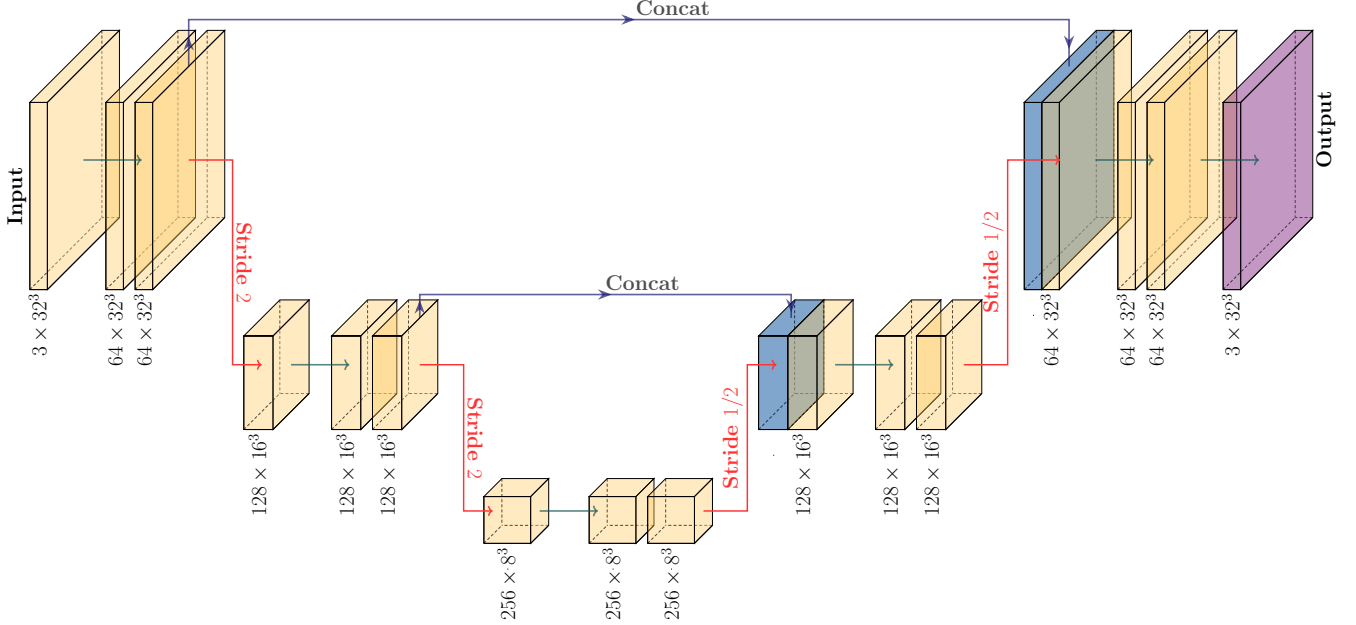


Figure 1. The plot shows our U-Net architecture. Each orange box corresponds to a multi-channel feature map. The number of channels and the output size is illustrated on the bottom of each box. The blue boxes denote the concatenated parts of the box during the upsampling and the purple box shows the output of the network. All the arrows operations, except the last one, refer to a series of convolution followed by batch normalization and ReLU. The last arrow operation indicates a $1 \times 1 \times 1$ convolution used to map 64 features to the final 3-D data.

padding, BN and ReLU. The expansive path includes two repeated expansion blocks each of which consists of one up-sampling convolution with stride 1/2 that halves the number of feature channels, a concatenation, and two successive convolutions with stride 1, each followed by zero padding, BN and ReLU. At the final layer, a $1 \times 1 \times 1$ convolution without padding is used to map 64 features to the final 3-D data. In total the network present 15 convolutional layers.

3.2. Training

We train our model using the displacement field defined as:

$$\vec{d} = \vec{x}_f - \vec{x}_i, \quad (1)$$

where \vec{x}_f is the final position of the particles (at redshift $z = 0$) and \vec{x}_i is the Lagrangian position of the same particles on a uniform grid. The input and target of the neural network is the displacement field from simulations without and with massive neutrinos, respectively.

Our benchmark model consists of the Zel'dovich approximation (hereafter ZA) applied to massive neutrino models. The ZA is a significantly faster approximation to full N-body simulations produced by first-order perturbation theory with neutrinos. The reason why we use the Zel'dovich approximation and not the second-order Lagrangian perturbation theory (2LPT), is because it is currently unknown how to predict 2LPT in massive neutrino models. In particular, there is no estimate for the two significant quantities, the second-order scale-dependent growth factor, and growth rate, necessary to calculate the 2LPT in presence of massive neutrinos.

We train our neural network by using the mean absolute error loss function that is given by the sum of all

the absolute differences between the target displacement field and the predicted values:

$$\mathbb{L} = \sum_{i=1}^N \left| \vec{d}_i^t - \vec{d}_i^p \right|, \quad (2)$$

where \vec{d}_i^t is the true displacement field (from massive neutrino simulations), \vec{d}_i^p is the prediction from the U-Net, and N is the total number of particles.

Table 1 presents the details of the Hyper-parameters used in our network. The total number of trainable parameters is 8.4×10^7 .

Hyper-parameter	Description	Value
lr	learning rate	10^{-4}
Epochs	number of epochs	3
Batch_size	batch size	64
Optimizer	optimizer for training	Adam
Regularization	L2 regularization of the loss function	10^{-4}

Table 1
Hyper-parameters used in the U-Net.

Figure 2 shows the projected density field of an N-body simulation with massive neutrinos at $z = 0$ (top panel), together with the residuals between the target and the input (bottom-left panel) and the output of our neural network (bottom-right panel). From the top panel, we can clearly see the presence of the filaments, surrounded by large underdense regions (dark regions), called voids, in between. The presence of massive neutrinos in the simulations induces a suppression in the growth of density perturbations on small scales, visible in the matter power spectrum. From the bottom panels, we can note

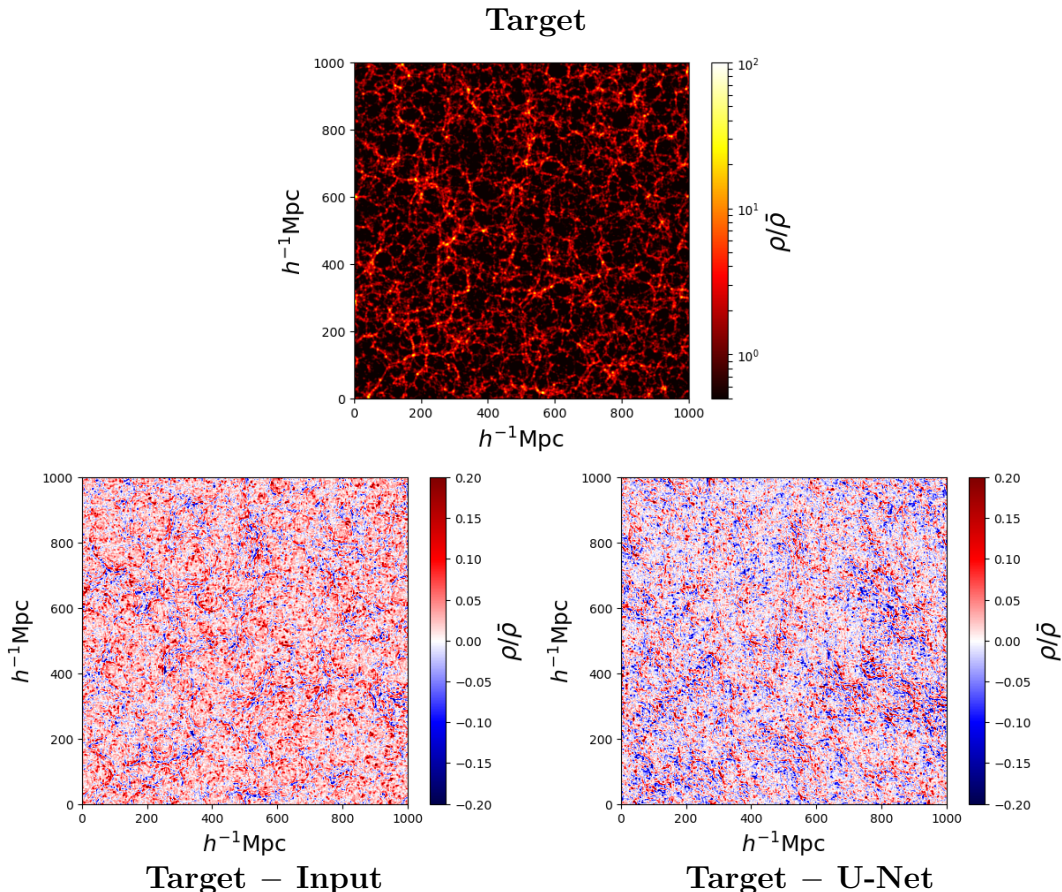


Figure 2. The top panel shows the cold dark matter density field at $z = 0$ from a region of $1000 \times 1000 \times 15$ $(h/\text{Mpc})^3$ for a massive neutrinos model ($M_\nu = 0.15$ eV). The bottom-left panel shows the residuals between the target (massive neutrino simulations) and the simulations with massless neutrinos (the input), while the bottom-right panel depicts the residual between the target and U-Net model. Notice that the residual is much smaller for the Target-U-Net than the Target-Input.

that the residuals between the target and the U-Net prediction (bottom-right panel) is smaller compared to the bottom-left panel. This indicates that our model is able to reproduce quite well simulations with massive neutrinos.

3.3. Training time

One standard cosmological simulation without neutrinos currently requires ~ 500 CPU hours to complete. The addition of massive neutrinos increases the simulation time to ~ 700 CPU hours. The key advantage of the approach we describe in this work is its ability to reduce the additional computational cost of producing massive neutrino simulations. In particular, it requires ~ 10 GPU hours to train and only few minutes to generate one simulation with massive neutrinos: a *substantial* gain in computing time compared to standard N-body techniques.

4. RESULTS

In this section, we present the main results obtained by using the U-Net architecture and compare it with the standard N-body simulations and the benchmark model. We quantify the agreement between our model and numerical simulations by considering four different summary statistics: the 1-D probability distribution function (PDF), the power spectrum, the bispectrum, and

the void size function. By doing this, we can compare the properties of the fully 3-dimensional density distributions. We compute the considered statistics by concatenating the sub-cubes of each of the ten realizations in the test data and calculating the mean summary statistics over ten simulations.

4.1. 1-D Probability distribution function

We compute the 1-D PDF of the cold dark matter for the N-body simulations and U-Net model prediction. We first place the particles on a grid with 512^3 cells, and we smooth the density field with a top-hat filter on a scale of 10 Mpc/h. We then calculate the 1-D PDF as the fraction of cells with overdensity lying within a given interval. The PDF provides information on the distribution of CDM overdensities in the cells.

The results are depicted in Figure 3, where we show the comparison of the 1-D PDF among the standard simulations (the input, red dashed-dotted line), massive neutrino simulations (the target, black dashed line) and our U-Net model (blue line). We can see the very good agreement between the U-Net model and the target.

4.2. Power Spectrum

The most widely used statistic in cosmology to extract information from cosmological observations is the 2-point correlation function $\xi(r)$, which is defined as the

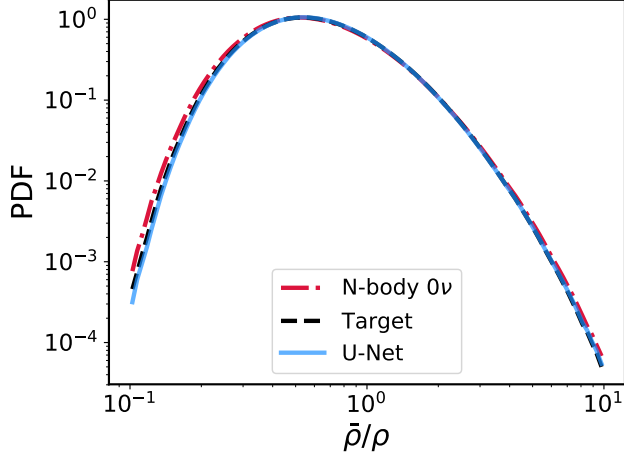


Figure 3. The normalized probability distribution function of CDM overdensities. The red and black lines show the 1-D PDF for N-body simulations with massless (the input of our U-Net) and massive neutrinos (target), respectively. The blue line depicts the U-Net results. Notice that the CNN model is able to reproduce very well the PDF from simulations with massive neutrinos.

excess probability, compared with a random distribution of galaxies, of finding a pair of galaxies at a given separation. The Fourier transform of the 2-point correlation function is the power spectrum, $P(k)$:

$$\begin{aligned} \xi(r) &= \langle \delta(\vec{r}') \delta(\vec{r}' + \vec{r}) \rangle \\ P(k) &= \int d^3\vec{r} \xi(r) e^{i\vec{k}\cdot\vec{r}}, \end{aligned} \quad (3)$$

where k is wavenumber of a fluctuation, that is related to the wavelength λ by $k = 2\pi/\lambda$. The power spectrum is the quantity predicted directly by theories for the formation of large-scale structure, and in the case of a Gaussian density field, it provides a complete statistical description of its fluctuations.

In order to quantify the performance of our model against the target, we compute the transfer function $T(k)$, defined as the square root of the ratio of the two power spectra:

$$T(k) = \sqrt{\frac{P_{\text{pred}}(k)}{P_{\text{target}}(k)}}, \quad (4)$$

where $P_{\text{pred}}(k)$ and $P_{\text{target}}(k)$ are the power spectra of the density field predicted by the U-Net model and the target, respectively.

Figure 4 shows the average power spectrum and the transfer function of the density field over ten simulations. The red and black lines on the top panel correspond to the power spectrum of N-body simulations without and with massive neutrinos. We note that massive neutrinos induce a suppression of the power spectrum at small scales (larger k). This is the most significant effect of neutrino masses on the several cosmological observables. Neutrinos, being hot thermal relics, possess large velocity dispersion. Consequently, the non-relativistic neutrino overdensities will only cluster at wavelengths larger than their free streaming wavenumber, reducing the growth of cold dark matter fluctuations on small scales.

The blue and green lines depict the power spectrum

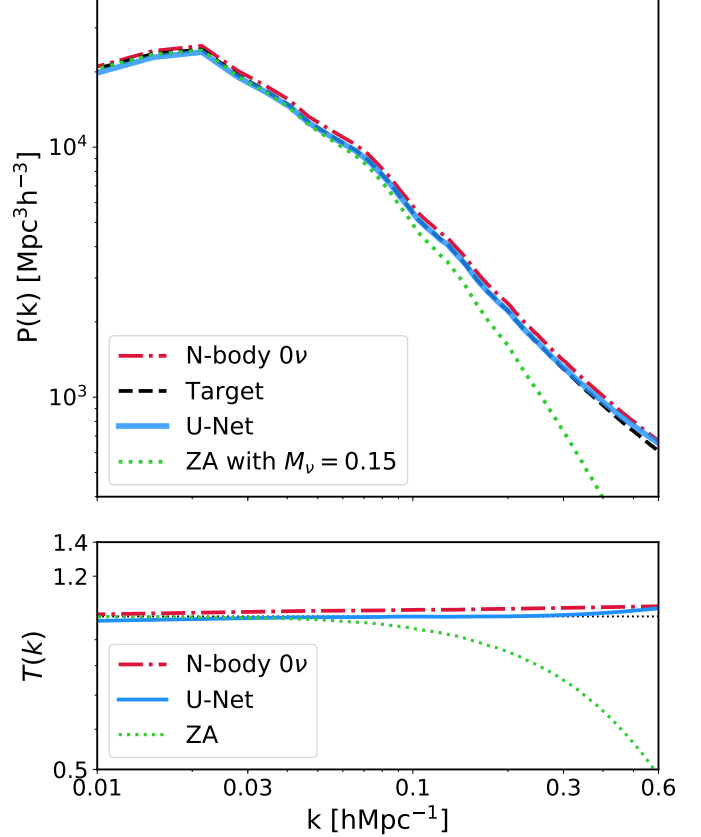


Figure 4. The top panel shows the matter power spectrum comparison among the standard N-body simulations (the input of the U-Net, red dashed-dotted line), massive neutrino simulations (the target, black dashed line), CNN model dubbed U-Net (blue line) and Zel'dovich approximation (the benchmark model, green dotted line). The bottom panel depicts the transfer function for the input, the U-Net and the benchmark model.

from the U-Net and benchmark model (Zel'dovich approximation). Notice that the latter reproduces the power spectrum accurately on very large-scales ($k < 0.05 h/\text{Mpc}$). This is what we expect since we are using the Zel'dovich approximation and not 2LPT (see subsection 3.2).

We find that the density distribution from the U-Net sample has, on large-scales an average power spectrum which is very close in amplitude and in shape to that of N-body simulations with neutrinos (the target). On smaller scales, the power spectrum of our model departs from that of the target. To quantify this deviation, we focus on the bottom panel of Figure 4, that shows the transfer function as a function of wavenumber for the benchmark model, the U-Net and the input. For an entirely accurate prediction, the transfer function is expected to be 1. The transfer function of the ZA approximation is close to one up to $k < 0.05 h/\text{Mpc}$ and then decreases as expected. On the other hand, the transfer function of the U-Net prediction is approximately 1 for $0.03 < k < 0.5 h/\text{Mpc}$ and differ from the unity by a 3.5% on scales $k \approx 0.55 h/\text{Mpc}$. This discrepancy increases to 6.3% as k increases around $0.7 h/\text{Mpc}$. Those results suggest that our model manages to predict the power spectrum accurately with massive neutrinos from large to

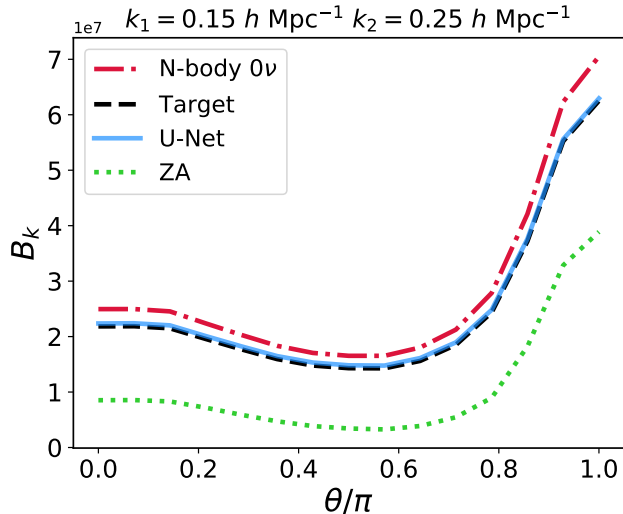


Figure 5. The plot shows the bispectrum predicted by standard Λ CDM simulations (the input of our architecture, red dashed-dotted line), massive neutrino simulations (the target, black dashed line), CNN model (blue line) and Zel’dovich approximation (the benchmark model, green dotted line). We set $k_1 = 0.15$ h/Mpc and $k_2 = 0.25$ h/Mpc. Notice that the bispectrum of the U-Net model is very close to that of the target.

intermediate scales. On smaller scales ($k > 0.7$ h/Mpc) the prediction starts to deviate from the target. This is not a surprise since those are the scales where the effects of non-linear evolution are important, and the mapping becomes highly non-trivial.

4.3. Bispectrum

The inflationary scenario predicts Gaussian initial conditions. The statistical properties of the Universe’s density field should be fully characterized by the 2-point correlation function (2PCF) or the power spectrum. However, on small scales, non-linear gravitational instability induces non-Gaussian signatures in the mass distribution, which contain information on the nature of gravity and the dark matter. The lowest order statistical tool to describe a non-Gaussian field is the three-point correlation function (3PCF), or equivalently, its Fourier transform, the bispectrum, defined as:

$$B(k_1, k_2, k_3) = \langle \delta_{\mathbf{k}_1} \delta_{\mathbf{k}_2} \delta_{\mathbf{k}_3} \rangle. \quad (5)$$

The bispectrum plays an important role in cosmology because it carries information about the spatial coherence of large-scale structures and can place strong constraints on models of structure formation. The presence of massive neutrinos induces a suppression of the amplitude of the bispectrum (Ruggeri et al. 2018). Furthermore, Hahn et al. (2019) have shown that the bispectrum is a powerful probe in constraining the total neutrino mass since can break the degeneracies between M_ν and the other cosmological parameters.

Figure 5 shows the average bispectrum over ten simulations for our U-Net model (blue line), the benchmark model (green line), the input (red line) and the target (black line). We have selected a value of $k_1 = 0.15$ h/Mpc, and of $k_2 = 0.25$ h/Mpc and varied the angle among those two vectors. Those scales correspond

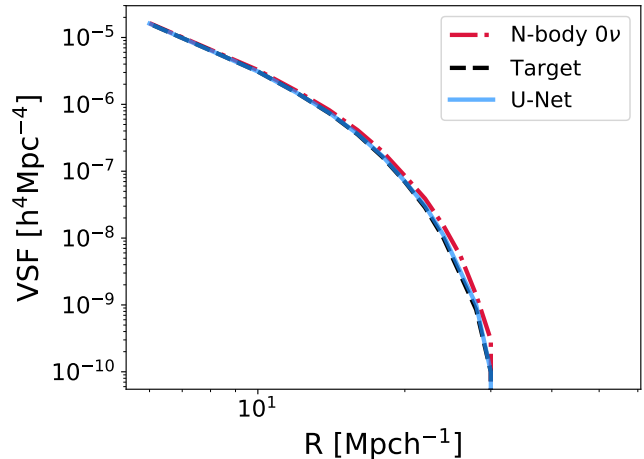


Figure 6. Void size function for the input (standard N-body simulations, red dashed-dotted line), target (massive neutrino simulations, black dashed line) and U-Net model (blue line). Notice that the U-Net is able to reproduce the void abundance from the target with very high accuracy.

to the maximum wavenumbers adopted in cosmology to infer the cosmological parameters from the galaxy power spectrum measurements.

We find that the mean relative bispectrum residual of our model compared to the target is 0.4%. This suggests that the U-Net model can generate neutrino simulations with correct higher-order statistics in the mildly non-linear regime. Notice that on the other hand, the benchmark model is not able to reproduce the bispectrum from the target. This is not surprising as the validity of the Zel’dovich approximation, will be limited to large scales.

4.4. Voids Abundance

Voids are the most under-dense regions of our Universe and together with halos, filaments, and walls, constitute the large-scale structure of the Universe, known as the cosmic web. Voids enclose a large amount of cosmological information since they fill most of the volume of the Universe. Massive neutrinos modify the properties of cosmic voids, such as their number, size and shape. This occurs because the large thermal velocities of massive neutrinos prevent their evacuation from cosmic voids. Consequently, such additional mass within voids affects their evolution.

The last statistical tool we consider in this section is the void size function, defined as the abundance of voids as a function of the voids radius. In presence of massive neutrinos, the abundance of large voids is suppressed. This occurs because the additional neutrino masses inside the voids slow down their evolution and make voids smaller and denser (Massara et al. 2015; Kreisch et al. 2019; Pisani et al. 2019). Here we used the algorithm described in Banerjee & Dalal (2016) in order to identify voids in the galaxy distribution of our U-Net model, the target and the input. In Figure 6, we compare the average void size function over ten realizations from the U-Net model (blue line), the input (red line), and the target (black line). We can see the suppression of the voids abundance induced by massive neutrinos (blue and black lines) at larger radius. We can also note the good agree-

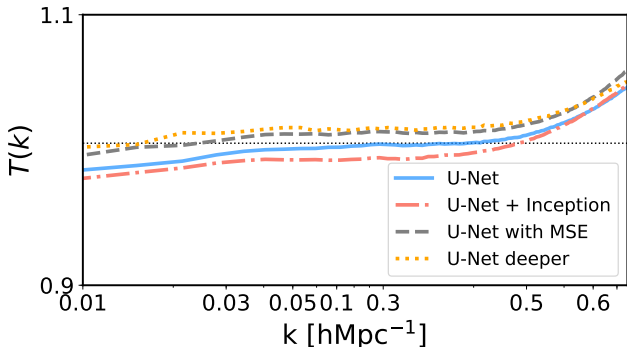


Figure 7. Transfer function comparison among the U-Net model (blue line) used in the analysis and the modified version of the architecture obtained by including the Inception module (pink dashed-dotted line), varying the loss function (grey dashed line) and increasing the number of layers (orange dotted line).

ment in the void size function among the U-Net model and the target. This indicates that our approach is also able to capture voids’ information completely.

4.5. Additional tests

Although our model reproduces the target within 6.3% up to scales $k \approx 0.7$ h/Mpc, the accuracy degrades on smaller non-linear scales. In order to improve the model efficiency at those scales, we perform some additional tests.

We first tune the hyperparameters in the neural network. In particular, we increase the number of the layers, change the learning rate and the batch size, and apply the mean square error (MSE) loss function.

We then test different convolutional neural network architectures. Specifically, we implement the U-Net by including an Inception module after the first block in the down-sampling and before the last block in the expansive path. The Inception network (Szegedy et al. 2014) uses convolutions of different sizes to capture details at varied scales. In our case, we are interested in extracting detailed features on smaller scales. This motivates the use of the Inception module at the beginning and at the end of the U-Net. In particular, we use the first original version of the Inception architecture with 3 different sizes of filters (1×1 , 3×3 , 5×5) and max pooling layers. The outputs are then concatenated and passed as input to the second/last block of the U-Net.

The results are depicted in Figure 7. We compare the transfer function of the additional tests we performed with the U-Net architecture used in our analysis. We can see that these tests do not significantly improve the performance of our model at smaller scales. We only find a slight improvement on larger scales when we consider the MSE loss function or a deeper U-Net architecture. This demonstrates the stability of our model and shows that more accurate trials are needed to improve the predictions on non-linear scales. We leave this exploration to future work.

5. CONCLUSIONS

Upcoming galaxy surveys, such as Euclid, DESI, DES or LSST, are expected to reach the sensitivity necessary to detect the absolute scale of neutrino masses. To achieve this goal, precise theory predictions are required

to analyze the data from those surveys and to understand and model the impact of non-linearities in the matter power spectrum, galaxy bias, and redshift space distortion in presence of massive neutrinos. A powerful way to obtain accurate theory predictions is by running numerical cosmological simulations. However, producing those simulations requires high computational resources.

In this work, we have presented a deep learning approach to predict fast non-standard cosmological simulations with massive neutrinos from standard N-body simulations. We have quantified the performance of our U-Net model by considering four summary statistics often used in cosmology: the 1-D PDF, the power spectrum, the bispectrum, and the void abundance. We have shown that our model is able to learn the mapping between the displacement field in simulations with massless and massive neutrinos, down to scales as small as 0.7 h/Mpc at $z = 0$, and reproduce the effect of massive neutrinos in large-scale structure. Moreover, with our method, we can generate massive neutrino simulations five orders of magnitude faster than the traditional methods and dramatically reduce the computational costs necessary of implementing simulations with massive neutrinos.

This work demonstrates that the deep learning approach is an accurate alternative to the traditional N-body techniques by mapping simulations with massive neutrinos directly from simulations with massless neutrinos. The use of such approach will be particularly useful in the near future. The need for fast N-body simulations will increase with the upcoming large cosmological surveys such as Euclid and LSST. Our methods will thus be crucial for producing fast and large simulation datasets for cosmological analyses.

In future work, we will improve our model to capture the effect of massive neutrinos on smaller non-linear scales by using the QUIJOTE high-resolution simulations (Villaescusa-Navarro et al. 2019). Another future direction will be to explore the possibility of generating fast neutrino simulations with an arbitrary mass from the standard Λ CDM simulations or more complex non-standard cosmological simulations that include, for example, modified gravity or primordial non-gaussianity effects.

We note that recently, Zennaro et al. (2019) has presented a new method to *rescale* massless neutrinos simulations to massive neutrinos simulations, following a very different approach to the one used in this work. Using the output of that method as the input of our neural net has the potential to improve the accuracy of both our method and Zennaro et al. (2019) results, as neural nets train faster on residuals. We plan to study this in future work.

ACKNOWLEDGEMENTS

We thank Gabriella Contardo, Elena Massara, Barnabas Pócosz, Siamak Ravanbakhsh, and David Spergel for useful discussions. EG acknowledges Nick Carriero from the Flatiron Institute for his help in solving technical problems with GPUs. The work of EG, FVN, SH and SH is supported by the Simons Foundation. The HADES and QUIJOTE simulations are publicly available at <https://franciscovillaescusa.github.io/hades.html> and <https://github.com/franciscovillaescusa/>

[Quijote-simulations](#), respectively. The analysis of the simulations and training of the neural network has been carried out in the Rusty cluster of the Flatiron Institute.

REFERENCES

- Abe, K., et al. 2014, *Phys. Rev. Lett.*, 112, 061802, [arXiv:1311.4750]
- Abe, Y. et al. 2012, *Phys. Rev. D*, 86, 52008, [arXiv:1207.6632]
- Adamson, P., et al. 2008, *Phys. Rev. Lett.*, 101, 131802, [arXiv:0806.2237]
- Ahmad, Q. R., et al. 2002, *Phys. Rev. Lett.*, 89, 011301, [arXiv:nucl-ex/0204008]
- Ahn, J. K., et al. 2012, *Phys. Rev. Lett.*, 108, 191802, [arXiv:1204.0626]
- Aker, M., et al. 2019, [arXiv:1909.06048]
- Araki, T., et al. 2005, *Phys. Rev. Lett.*, 94, 081801, [arXiv:hep-ex/0406035]
- Banerjee, A., & Dalal, N. 2016, *J. Cosmology Astropart. Phys.*, 2016, 015, [arXiv:1606.06167]
- Bel, J., Pezzotta, A., Carbone, C., Sefusatti, E., & Guzzo, L. 2019, *Astron. Astrophys.*, 622, A109, [arXiv:1809.09338]
- Bird, S., Viel, M., & Haehnelt, M. G. 2012, *Mon. Not. Roy. Astron. Soc.*, 420, 2551, [arXiv:1109.4416]
- Castorina, E., Carbone, C., Bel, J., Sefusatti, E., & Dolag, K. 2015, *JCAP*, 1507, 043, [arXiv:1505.07148]
- Castorina, E., Sefusatti, E., Sheth, R. K., Villaescusa-Navarro, F., & Viel, M. 2014, *J. Cosmology Astropart. Phys.*, 2, 049, [arXiv:1311.1212]
- Esteban, I., Gonzalez-Garcia, M. C., Maltoni, M., Martinez-Soler, I., & Schwetz, T. 2017, *J. High Energy Phys.*, [arXiv:1611.01514]
- Forero, D. V., Tórtola, M., & Valle, J. W. 2014, *Phys. Rev. D - Part. Fields, Gravit. Cosmol.*, [arXiv:1405.7540]
- Fukuda, Y., et al. 1998, *Phys. Rev. Lett.*, 81, 1562, [arXiv:hep-ex/9807003]
- Giusarma, E., Gerbino, M., Mena, O., Vagnozzi, S., Ho, S., & Freese, K. 2016, *Phys. Rev.*, D94, 083522, [arXiv:1605.04320]
- Giusarma, E., Vagnozzi, S., Ho, S., Ferraro, S., Freese, K., Kamen-Rubio, R., & Luk, K.-B. 2018, *Phys. Rev.*, D98, 123526, [arXiv:1802.08694]
- Gonzalez-Garcia, M. C., Maltoni, M., & Schwetz, T. 2014, *JHEP*, 11, 052, [arXiv:1409.5439]
- Hahn, C., Francisco, V.-N., Emanuele, C., & Roman, S. 2019, [arXiv:1909.11107]
- He, S., Li, Y., Feng, Y., Ho, S., Ravanbakhsh, S., Chen, W., & Póczos, B. 2019, *Proc. Nat. Acad. Sci.*, 116, 13825, [arXiv:1811.06533]
- He, S., Ravanbakhsh, S., & Ho, S. 2018, *Analysis of Cosmic Microwave Background with Deep Learning*
- Hezaveh, Y. D., Perreault Levasseur, L., & Marshall, P. J. 2017, *Nature*, 548, 555, [arXiv:1708.08842]
- Kraus, C., et al. 2005, *Eur. Phys. J.*, C40, 447, [arXiv:hep-ex/0412056]
- Kreisch, C. D., Pisani, A., Carbone, C., Liu, J., Hawken, A. J., Massara, E., Spergel, D. N., & Wandelt, B. D. 2019, *Mon. Not. Roy. Astron. Soc.*, 488, 4413, [arXiv:1808.07464]
- Krizhevsky, A., Sutskever, I., & Hinton, G. E. 2012, in *Advances in Neural Information Processing Systems 25*, ed. F. Pereira, C. J. C. Burges, L. Bottou, & K. Q. Weinberger (Curran Associates, Inc.), 1097–1105
- Lesgourgues, J., & Pastor, S. 2012, *Adv. High Energy Phys.*, 2012, 608515, [arXiv:1212.6154]
- Massara, E., Villaescusa-Navarro, F., Viel, M., & Sutter, P. M. 2015, *J. Cosmology Astropart. Phys.*, 11, 018, [arXiv:1506.03088]
- Palanque-Delabrouille, N. et al. 2015, *J. Cosmol. Astropart. Phys.*, 2015, 11, [arXiv:1506.05976]
- Peloso, M., Pietroni, M., Viel, M., & Villaescusa-Navarro, F. 2015, *JCAP*, 1507, 001, [arXiv:1505.07477]
- Pisani, A., et al. 2019, [arXiv:1903.05161]
- Planck Collaboration, Aghanim, N. et al. 2019, *arXiv e-prints*, [arXiv:1907.12875]
- Planck Collaboration, Akrami, Y. et al. 2018, *arXiv e-prints*, [arXiv:1807.06205]
- Ravanbakhsh, S., Oliva, J., Fromenteau, S., Price, L. C., Ho, S., Schneider, J., & Póczos, B. 2017, *arXiv:1711.02033 [astro-ph, stat]*, [arXiv:1711.02033]
- Rodriguez, A. C., Kacprzak, T., Lucchi, A., Amara, A., Sgier, R., Fluri, J., Hofmann, T., & Réfrégier, A. 2018, *Comput. Astrophys. Cosmol.*, 5, 4, [arXiv:1801.09070]
- Ronneberger, O., Fischer, P., & Brox, T. 2015, *Lect. Notes Comput. Sci. (including Subser. Lect. Notes Artif. Intell. Lect. Notes Bioinformatics)*
- Ruggeri, R., Castorina, E., Carbone, C., & Sefusatti, E. 2018, *JCAP*, 1803, 003, [arXiv:1712.02334]
- Szegedy, C. et al. 2014, *CoRR*, abs/1409.4842, [arXiv:1409.4842]
- Vagnozzi, S., Giusarma, E., Mena, O., Freese, K., Gerbino, M., Ho, S., & Lattanzi, M. 2017, *Phys. Rev. D*, 96, 123503, [arXiv:1701.08172]
- Villaescusa-Navarro, F., Banerjee, A., Dalal, N., Castorina, E., Scocimarro, R., Angulo, R., & Spergel, D. N. 2018, *Astrophys. J.*, 861, 53, [arXiv:1708.01154]
- Villaescusa-Navarro, F. et al. 2019, *arXiv e-prints*, [arXiv:1909.05273], [arXiv:1909.05273]
- Villaescusa-Navarro, F., Marulli, F., Viel, M., Branchini, E., Castorina, E., Sefusatti, E., & Saito, S. 2014, *J. Cosmology Astropart. Phys.*, 3, 011, [arXiv:1311.0866]
- Villaescusa-Navarro, F., Vogelsberger, M., Viel, M., & Loeb, A. 2013, *Mon. Not. Roy. Astron. Soc.*, 431, 3670, [arXiv:1106.2543]
- Zamudio-Fernandez, J., Okan, A., Villaescusa-Navarro, F., Bilaloglu, S., Cengiz, A. D., He, S., Perreault Levasseur, L., & Ho, S. 2019, [arXiv:1904.12846]
- Zennaro, M., Angulo, R. E., Aricò, G., Contreras, S., & Pellejero-Ibáñez, M. 2019, [arXiv:1905.08696]
- Zennaro, M., Bel, J., Dossett, J., Carbone, C., & Guzzo, L. 2018, *Mon. Not. Roy. Astron. Soc.*, 477, 491, [arXiv:1712.02886]